

Equilibrium and kinetics studies of hexavalent chromium biosorption on a novel green macroalgae *Enteromorpha* sp.

S. Rangabhashiyam¹ · E. Suganya¹ · Alen Varghese Lity¹ · N. Selvaraju¹

Received: 8 February 2015 / Accepted: 28 April 2015 / Published online: 8 May 2015
© Springer Science+Business Media Dordrecht 2015

Abstract This study focuses on the use of novel *Enteromorpha* sp. macroalgal biomass (EMAB), for the biosorption of hexavalent chromium from aqueous solutions. The biosorbent was characterized by Fourier transformer infrared spectroscopy, energy dispersive spectroscopy, and scanning electron microscopy techniques. The effect of experimental parameters such as pH, initial concentration of Cr(VI) ions, biosorbent dosage, and temperature were evaluated. The maximum biosorption capacity for Cr(VI) was observed at pH 2.0. The modeling of the experimental data at equilibrium was performed using two parameter isotherm models. Both Langmuir and Freundlich isotherm equations better fitted the equilibrium data. A contact time of different initial Cr(VI) concentrations was about 160 min to attain biosorption equilibrium. The kinetic data were fitted by models including pseudo-first-order, pseudo-second-order, and intraparticle diffusion. The pseudo-second-order and intraparticle diffusion kinetic models adequately described the kinetic data. Moreover, the thermodynamic parameters indicated that the biosorption process was spontaneous, endothermic, and increased randomness in nature. The results showed that EMAB could be used as an effective biosorbent for the removal of Cr(VI) from aqueous solution.

Keywords Biosorption · Green macroalgae · Hexavalent chromium · Seaweed · Toxicity · Wastewater treatment

✉ N. Selvaraju
selvaraju@nitc.ac.in

¹ Department of Chemical Engineering, National Institute of Technology Calicut, Kozhikode 673601, Kerala, India

List of symbols

A_T	Temkin isotherm equilibrium binding constant (L mg^{-1})
b_T	Temkin isotherm constant (J mol^{-1})
b_L	Langmuir isotherm constant (L mg^{-1})
C_0	Initial Cr(VI) concentration (mg L^{-1})
C_e	Cr(VI) concentration in solution at equilibrium (mg L^{-1})
E	Mean biosorption energy E (kJ mol^{-1})
K_F	Freundlich constant (L g^{-1})
K	Dubinin–Radushkevich model constant ($\text{mol}^2 \text{kJ}^{-2}$)
K_j	Jovanovic isotherm constant (L g^{-1})
k_1	Pseudo-first-order rate constant (min^{-1})
k_2	Pseudo-second-order rate constant ($\text{g mg}^{-1} \text{min}^{-1}$)
k_{id}	Intraparticle diffusion rate constant ($\text{mg g}^{-1} \text{min}^{-1/2}$)
k_c	Equilibrium constant
m	Amount of biosorbent (g)
n_F	Freundlich exponent
Q_0	Monolayer coverage capacity (mg g^{-1})
Q_m	Maximum adsorption capacity (mg g^{-1}) in Dubinin–Radushkevich model
q_{mj}	Maximum adsorption capacity in Jovanovic model (mg g^{-1})
q_e	Amount of Cr(VI) ions adsorbed per unit mass of biosorbent (mg g^{-1})
R	Gas constant ($8.314 \text{ J mol}^{-1} \text{ K}^{-1}$)
R_L	Separation factor
V	Volume of the solution (L)
ΔG°	Gibbs free energy (kJ mol^{-1})
ΔH°	Enthalpy (kJ mol^{-1})
ΔS°	Entropy ($\text{J mol}^{-1} \text{ K}^{-1}$)
ε	Polanyi potential

Introduction

Effluents generated from industrial sources of electrolytic treatment, ceramic production, fertilizer production, pigments production, steel manufacturing sectors, etc., can cause heavy metal contamination [1]. The toxic metal ions are non-degradable in nature, and their persistence will lead to bioaccumulation and biomagnifications through the food chain entry [2–4]. Hexavalent chromium, because of the potential toxicity effects, has been considered as the 16th toxic contaminant [5]. Toxicity of hexavalent chromium is mainly due to the negatively charged chromate and dichromate anion complex that affects the normal sulfate ionic channels and results in the formation of various detrimental reactive intermediates [6]. Chromium is present in the industrial effluents from aluminum, ink, dye, steel, textile, paint, electroplating industries, and the tannery wastewater primarily as trivalent and hexavalent forms. Trivalent chromium is relatively less toxic and less mobile than hexavalent chromium [7, 8]. But hexavalent chromium causes dermatitis, chronic ulcers, nasal septum perforation, lung cancer, and damage

to the kidneys, liver, and gastric tract [9]. The World Health Organization Standard's recommended guideline value for total chromium in drinking water as 0.05 mg L^{-1} . The permissible limit for hexavalent chromium release into inland surface water is 0.1 mg L^{-1} [10–12]. Therefore, treatment of the effluents before discharge of hexavalent chromium into aquatic environments is highly indispensable.

Different conventional technologies like ion exchange, evaporative recovery, coagulation, chemical precipitation, reverse osmosis, filtration, membranes, and adsorption by activated carbon have been employed to eliminate Cr(VI) from industrial wastewater. However, these methods have economic constraints and are ineffective especially when the Cr(VI) concentration is in the range of $1\text{--}100 \text{ mg L}^{-1}$ [13, 14]. In this context, biosorption has emerged as an alternative technique with the merits of being technically simple, eco-friendly, recyclable, using a minimal volume of sludge generation, and highly economical [15, 16]. Biosorption is a physico-chemical and metabolically independent process intended for the removal of Cr(VI) by subjecting biosorbents from different biological materials sources like microorganisms, seaweeds, plant biomass, industrial wastes, agricultural residues, etc. [17]. The biosorbents contain biomolecules such as the polysaccharides, proteins, etc., with specific functional groups, which are mainly responsible for Cr(VI) biosorption [18]. Different types of biosorbents such as, *Laminaria japonica* [19], *Undaria pinnatifida* [19], *Porphyra haitanensis* [19], *Gracilaria lemaneiformis* [19], *Halimeda gracilis* [20], *Sterculia guttata* shell [21], Maize corn cob [9], *Ulva lactuca* [22], etc., have been investigated for the removal of Cr(VI).

In the present investigation, the raw form of EMAB was employed for the biosorption of Cr(VI) from the aqueous solution. The influence of different experimental parameters such as initial solution pH, biosorbent dosage, initial Cr(VI) concentration, and temperature on Cr(VI) biosorption by EMAB was evaluated. Moreover, isotherms, kinetics, and thermodynamic modeling were performed in order to predict the feasibility of EMAB for the removal of hexavalent chromium from the aqueous solution.

Materials and methods

Preparation of biosorbent

Enteromorpha sp. green marine macroalgae was collected from coastal area of the Kozhikode, India. The collected EMAB was washed in running tap water followed by Milli-Q water to eradicate surface interfering ions and other undesired materials like sand particles and debris from its surface. The EMAB was then sun dried for 5 days followed by drying in an oven at 343 K for 40 min. Subsequently, EMAB was ground on a laboratory blender and sieved, to select the particles size between 0.125 and 0.250 mm. The prepared EMAB was stored in an air tight plastic container for further use without any pre-treatment. The lignin, cellulose, and hemicelluloses constituents of EMAB were evaluated according to Moubasher et al.

Table 1 Physical and chemical properties of the EMAB sample

Parameters	Values
Cellulose (%)	30.57
Hemicellulose (%)	23.7
Lignin (%)	2.4
Moisture (%)	12.2
Ash content (%)	15
pH	6.2
pH _{ZPC}	6.5
Conductivity (mS cm ⁻¹)	1.790
Particle size (mm)	0.125–0.250

[23], the remaining parameters of Table 1 were determined according to Nama-sivayam et al. [24].

Preparation of synthetic wastewater

The standard 1000 mg L⁻¹ of Cr(VI) stock solution was prepared and further diluted to obtain the required initial concentration in the range of 20–100 mg L⁻¹ Cr(VI) solutions. The pH of the solutions was adjusted using 0.1 M NaOH and 0.1 M HCl after addition of the biosorbent.

Characterization of EMAB

A scanning electron microscope (JSM-6390LV, Jeol) was used to observe the surface morphology of the biosorbent. Energy-dispersive X-ray spectroscopy (JED-2300, Jeol) was carried out to examine the elements distribution on the EMAB surface. FTIR studies were performed to determine the type of functional group responsible for the Cr(VI) biosorption (Nicolet Avatar 370; Thermo Scientific). Percentages of the elements C, H, and N in the EMAB were determined using a C–H–N Analyzer (Vario EL III, Elementar). The EMAB surface area was determined through a surface area analyzer (ASAP 2200, Micromeritics).

Batch biosorption studies

The biosorption of hexavalent chromium on the EMAB was investigated in batch mode operation. The effects of experimental parameters like solution pH (range 2.0–7.0), biosorbent dose (0.2–1.0 g L⁻¹), initial Cr(VI) concentration (20–100 mg L⁻¹), and temperature (303, 313, 323 and 333 K) had on the biosorption of Cr(VI) using EMAB were analyzed. The experimental studies were carried out in a 250 mL stoppered conical flask with the total volume of 50 mL solution, stirred on a thermostated shaking incubator (116736GB, GeNei). At the end of each experiment, the flasks were removed from the shaker and the solutions were separated from the biosorbent by filtration using Whatman No. 41 filter paper. The concentration of unadsorbed Cr(VI) ions in the reaction medium was

determined spectrophotometrically at 540 nm using a double beam UV–visible spectrophotometer (2201, Systronics) after complexation with 1,5-diphenylcarbazide in an acidic medium [25]. The biosorption capacity q_e (mg g^{-1}) was calculated using the below equation.

$$q_e = \frac{(C_0 - C_e) \times V}{m}, \quad (1)$$

where C_0 and C_e are the initial and equilibrium concentration of Cr(VI) ion in mg L^{-1} , V is the volume of Cr(VI) solution (L), and m is the mass of EMAB (g).

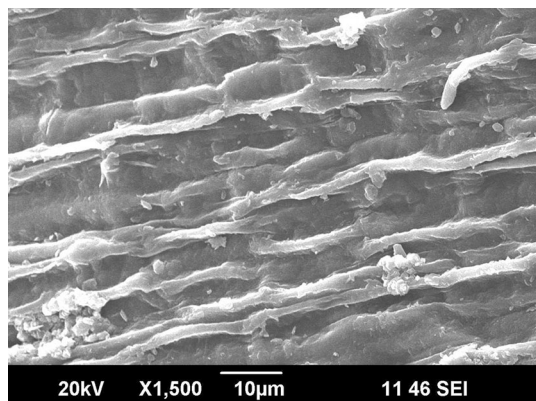
Results and discussion

Characterization of the biosorbent

The physico-chemical characteristics of EMAB were presented in Table 1. The elemental composition of EMAB was found to be 29.74 % C, 5.09 % H, 3.33 % S, and 1.65 % N. The BET surface area of EMAB was obtained as $3.6002 \text{ m}^2 \text{ g}^{-1}$. It was observed (Fig. 1) that the EMAB has smooth surface areas with grooves, regular ridges, and channels, which appeared highly dilated due to the presence of intermittently spaced protrusions that favor Cr(VI) biosorption. The EDS spectra of EMAB, Cr(VI) biosorbed EMAB, are shown in Fig. 2a, b, respectively. From the spectra, it has been concluded that Cr(VI) ions have been biosorbed on the surface of the EMAB.

The FTIR spectral analysis is significant in order to identify the characteristic functional groups responsible for biosorption of Cr(VI) ions (Fig. 3a, b). The major shift of biosorption peaks have been observed in the frequencies of 1633.34, 1423.53, 1229.20, 1048.97, and 599.43 cm^{-1} . Some peaks below 1000 cm^{-1} are referred to as the fingerprint zone. The fingerprint zone could be attributed to the phosphate or sulphur groups and aromatic –CH stretching vibrations [26, 27]. The

Fig. 1 SEM micrograph of EMAB



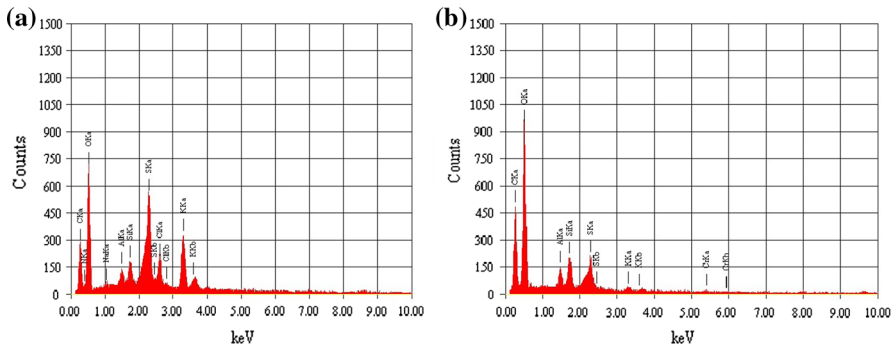


Fig. 2 EDS analysis of EMAB. **a** Before and **b** after Cr(VI) biosorption

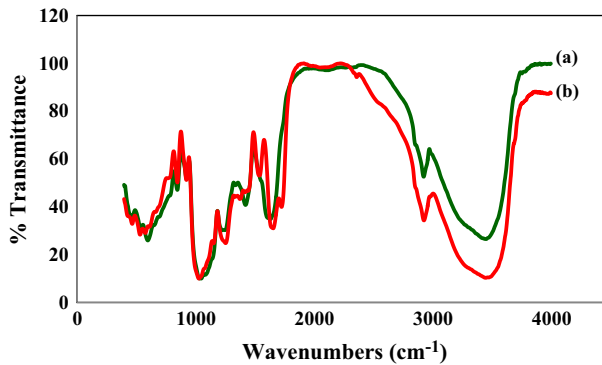


Fig. 3 FTIR spectra of EMAB. **a** Before and **b** after Cr(VI) biosorption

Table 2 Surface functional groups observed on EMAB before and after Cr(VI) biosorption using FTIR spectroscopy

Band position (cm^{-1})			Functional groups
Before biosorption	After biosorption	Differences	
3452.85	3450.83	-2.02	-OH and -NH ₂ stretching vibrations
2926.51	2928.77	2.26	Aliphatic C-H groups
	1728.03	94.69	
1633.34	1657.83	24.49	-NH ₂ bending vibration
1423.53	1540.43	116.9	Stretching vibration of C-O
1229.20	1255.91	26.71	C-O stretching
1048.97	1030.34	-18.63	Skeletal vibration of C-O

respective functional groups of these peak frequencies have been represented in Table 2. The differences in the FTIR spectra of EMAB before and after Cr(VI) biosorption confirm the binding of Cr(VI) ion with functional groups present on the EMAB.

Influence of solution pH on Cr(VI) biosorption

The initial pH of the biosorption system is an important parameter in the removal of hexavalent chromium [28]. In the present investigation, the effect of initial pH on the Cr(VI) biosorption using EMAB was studied in the initial pH range of 2.0–7.0. The plot of metal biosorption capacity (mg g^{-1}) versus pH is shown in Fig. 4. It is observed from the graph that the maximum biosorption by the EMAB is observed at pH 2.0. Increase in pH from 3.0 to 7.0 decreased the biosorption of Cr(VI) uptake by the EMAB. Maximum Cr(VI) biosorption capacity of 2.7795 mg g^{-1} was observed at pH 2.0, and this was due to the net positive charge on EMAB surface, which nevertheless decreased the biosorption capacity of 0.0161 mg g^{-1} that was obtained at pH 7.0. A similar result of hexavalent chromium removal using *Oedogonium hatei* was reported with the optimal pH of about 2.0 [29]. Based on the initial pH of the system, chromium is exhibited in various types. At pH of <2 , $\text{Cr}_3\text{O}_{10}^{2-}$, and $\text{Cr}_4\text{O}_{13}^{2-}$ species are formed; at the pH range of 2.0–6.0, HCrO_4^- , and $\text{Cr}_2\text{O}_7^{2-}$ ions are in equilibrium. When the pH of above 8, CrO_4^{2-} is the predominant species in the solution [30, 31]. The point of zero charge (pH_{pzc}) was determined by the solid addition method [32] and is reported in Table 1. It can be inferred from Fig. 5, the point of zero charge (pH_{pzc}) of the EMAB is found as 6.5. The surface charge of the EMAB was positively charged (attracting anions) at a pH value of <6.5 and negatively charged (repelling anions) are exhibited at the pH value of >6.5 .

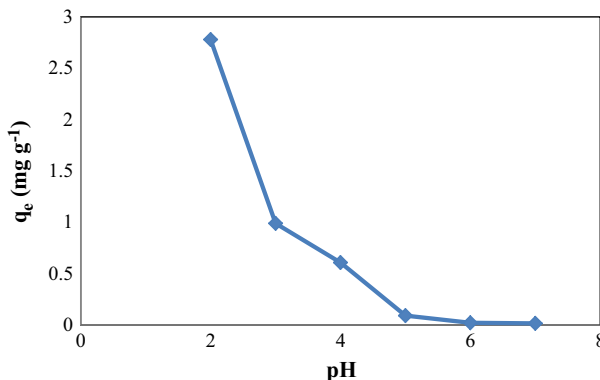


Fig. 4 Effect of pH on the biosorption of Cr(VI) at initial Cr(VI) concentration of 20 mg L^{-1} , biosorbent dose of 0.2 g, and temperature of 303 K

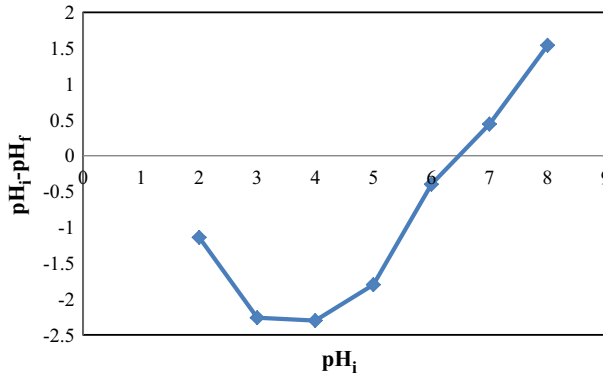


Fig. 5 Point of zero charge

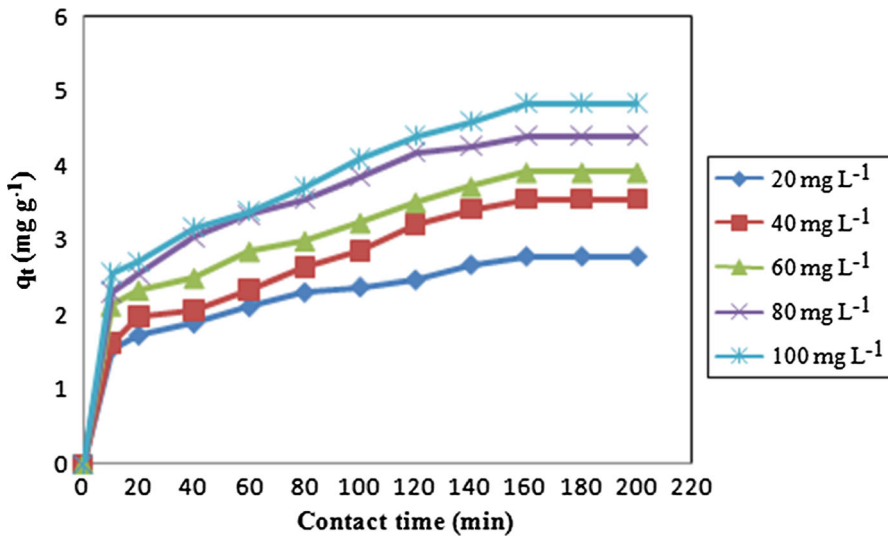


Fig. 6 Effect of contact time on the biosorption of different initial concentrations of Cr(VI) using 0.2 g of EMAB, at pH 2.0 and temperature of 303 K

Influence of contact time and initial Cr(VI) concentration

The effect of contact time on Cr(VI) biosorption on EMAB was investigated at different initial Cr(VI) concentrations ranging from 20 to 100 mg L⁻¹. Equilibrium time for the biosorption of Cr(VI) on EMAB at various Cr(VI) concentrations was found to be 160 min, which showed that equilibrium time was independent of initial metal ion concentration. The curves shown in Fig. 6 indicate single smooth and continuous action signifying the monolayer formation of Cr(VI) ion on the biosorbent surface. Cr(VI) uptake (mg g⁻¹) of the biosorbent increased from 2.7795

to 4.8387 mg g^{-1} as the initial Cr(VI) concentration increased from 20 to 100 mg L^{-1} . This is because, as the Cr(VI) ion to the biosorbent ratio increases, the higher energy sites are saturated and biosorption begins on lower energy sites, resulting in a decrease in the biosorption capacity of the biosorbent [33, 34].

Influence of biosorbent dose on Cr(VI) biosorption

The effect of EMAB dosage on the biosorption of Cr(VI) ions was investigated using six different biosorbent dosages at 20 mg L^{-1} initial Cr(VI) concentration. Biosorption capacity is defined as the mass of Cr(VI) ions biosorbed per unit mass of EMAB. If the EMAB dosage is increased at constant Cr(VI) concentration, the amount of Cr(VI) biosorbed per unit mass of EMAB decreases due to the availability of a lesser number of Cr(VI) ions. The results are presented in Fig. 7, the maximum biosorption capacity is observed as 2.7795 mg g^{-1} using 0.2 g L^{-1} EMAB dosage. This result may be attributed to the fact that the higher biosorbent dosage makes available the more biosorbent surface area and pores volume, which will be available for biosorption, but at lower optimal biosorbent dosage, all types of sites are entirely exposed and the biosorption on the surface is saturated faster, showing a higher biosorption capacity [15, 35, 36].

Influence of temperature on Cr(VI) biosorption

The effect of temperature on biosorption of Cr(VI) on EMAB was investigated by testing different temperatures from 303 to 333 K. Temperature affects the interaction between the biosorbent and the metal ions through influencing the metal–biosorbent complex stability and ionization of the cell wall moieties. The temperature of the biosorption solution could be vital for energy dependent mechanisms involved in the metal binding process [37]. Results presented in Fig. 8 indicate that the biosorption capacity of EMAB towards Cr(VI) removal was increased from 2.7795 to 4.9602 mg g^{-1} with the increase in temperature from 303

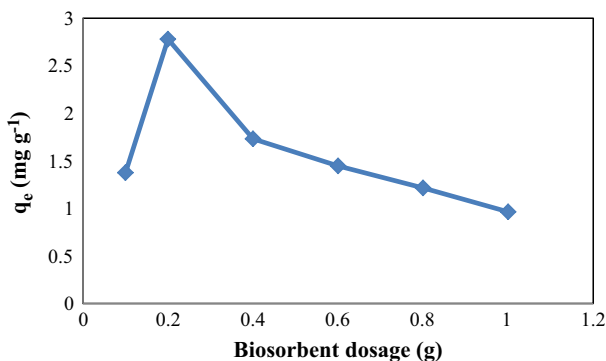


Fig. 7 Effect of biosorbent dose on the biosorption of Cr(VI) at initial Cr(VI) concentration of 20 mg L^{-1} , temperature of 303 K, and pH 2.0

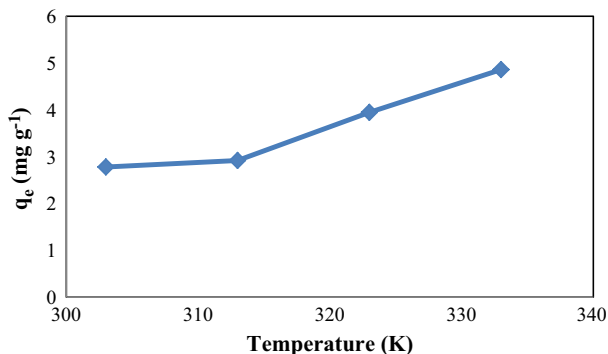


Fig. 8 Effect of temperature on the biosorption of Cr(VI) at initial Cr(VI) concentration of 20 mg L⁻¹, 0.2 g of biosorbent and pH 2

to 333 K, illustrating that Cr(VI) biosorption onto EMAB was an endothermic process. The increase in biosorption capacity with an increase in temperature may be because of the formation of new biosorption sites on EMAB or the increased kinetic energy of the Cr₂O₇²⁻ ion, the dominant form of chromium under acidic conditions [38].

Modeling of biosorption isotherms

One of the significant features for the evaluation of the biosorption process is the equilibria of biosorption. The equilibrium of biosorption of metal ions is modeled using biosorption isotherm equations. The biosorption isotherm equations were used to illustrate the experimental data and the thermodynamic assumptions of the models often provide some insight into the biosorption mechanism, the surface properties, and affinity of the biosorbent [39, 40]. The isotherm models like Langmuir, Freundlich, Dubinin–Radushkevich, Temkin, and Jovanovic were used to analyze the equilibrium data obtained in the present study.

Langmuir isotherm

The Langmuir isotherm equation is based on monolayer biosorption onto a surface with a finite number of identical sites, which are homogeneously distributed over the biosorbent surface [41]. The Langmuir model takes the form of the following equation

$$q_e = \frac{Q_0 K_L C_e}{1 + K_L C_e}, \quad (2)$$

where C_e is the equilibrium concentration (mg L⁻¹), q_e denotes the biosorption capacity (mg g⁻¹), Q_0 represents the maximum metal biosorption (mg g⁻¹), and K_L is the Langmuir isotherm constant (L mg⁻¹). The values of Q_0 and K_L were calculated from the slope and intercept of the linear plot (Fig. 9a) and were found to be

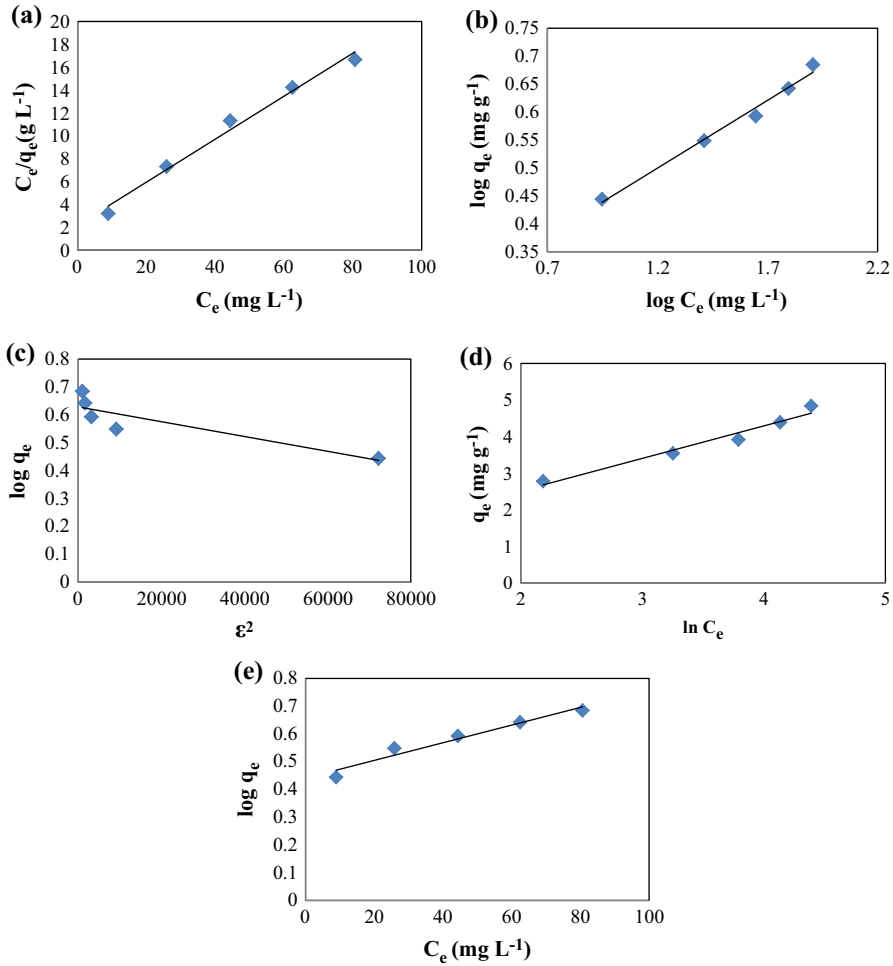


Fig. 9 Plots of **a** Langmuir, **b** Freundlich, **c** Dubinin–Radushkevich, **d** Temkin, and **e** Jovanovic isotherms for the biosorption of Cr(VI) onto EMAB

5.3475 mg g⁻¹ and 0.085 L mg⁻¹ as shown in Table 3. A comparison of biosorption capacity of EMAB with other biosorbents available in literature is presented in Table 7. In the Langmuir model, the biosorption intensity or dimensionless constant separation factor (R_L) is expressed by the following equation:

$$R_L = \frac{1}{1 + K_L C_0}, \tag{3}$$

where C_0 represent the initial metal concentration (mg L⁻¹). The conditions based on R_L values on biosorption are suggested as, $0 < R_L < 1$ for favorable, $R_L > 1$ for unfavorable, $R_L = 1$ for linear, and $R_L = 0$ for irreversible, respectively. The R_L

Table 3 Isotherm constants for biosorption of Cr(VI) onto EMAB

Models	Parameters	EMAB	Coefficient of determination (R^2)
Langmuir	Q_0 (mg g ⁻¹)	5.3475	0.985
	K_L (L mg ⁻¹)	0.085	
Freundlich	K_F (mg ^{1-1/n} L ^{1/n} g ⁻¹)	1.6143	0.986
	n_F	4.1322	
Dubinin–Radushkevich	Q_m (mg g ⁻¹)	4.2461	0.777
	K (mol ² J ⁻²)	3×10^{-6}	
	E (kJ mol ⁻¹)	0.4082	
Temkin	A_T (L mg ⁻¹)	1.0008	0.961
	b_T (kJ mol ⁻¹)	2.840	
Jovanovic	q_{mj} (mg g ⁻¹)	1.5542	0.954
	K_j (L g ⁻¹)	-0.003	

Table 4 Langmuir dimensionless constant separation factor for EMAB

Initial Cr(VI) concentration (mg L ⁻¹)	R_L value
20	0.3703
40	0.2272
60	0.1639
80	0.1282
100	0.1052

values for each of the different initial Cr(VI) concentrations used are between 0 and 1 confirmed viability of Cr(VI) biosorption onto EMAB (Table 4).

Freundlich isotherm

The Freundlich equation is the empirical relationship based on the assumption that the biosorption energy of the metal binding site on a biosorbent depends on whether the adjacent sites are already occupied or not. The limitation of this model is that the amount of biosorbed solute increases indefinitely with the concentration of solute in the solution [42]. The Freundlich equation is written as follows

$$q_e = K_F C_e^{1/n_F}, \quad (4)$$

where K_F (L g⁻¹) is the Freundlich constant and n_F is the Freundlich exponent. Values of $n_F > 1$ demonstrate the favorable nature of the biosorption process [43]. This model assumed that the stronger binding sites are occupied first. The plot of $\log q_e$ versus $\log C_e$ for the biosorption of Cr(VI) onto dried EMAB (Fig. 9b) was employed to generate the intercept value of K_F and the slope of $1/n_F$. Examination of the coefficient of determination reported in Table 4 shows that the experimental

data fitted well to the Freundlich model. The n_F value of 4.1322 was higher than 1.0, indicating favorable biosorption of Cr(VI) onto EMAB. Furthermore, the K_F value of 1.6143 indicates the easy uptake of Cr(VI) from aqueous solution by EMAB.

Dubinin–Radushkevich isotherm

The Dubinin–Radushkevich model envisages the heterogeneity of the surface energies [44]. This model in its nonlinear form is given as follows

$$q_e = Q_m \exp^{-K\varepsilon^2} \quad (5)$$

$$\varepsilon = RT \ln \left(1 + \frac{1}{C_e} \right), \quad (6)$$

where Q_m and K are the Dubinin–Radushkevich isotherm constants in mg g^{-1} and $\text{mol}^2 \text{J}^{-2}$, respectively. The ε , the Polanyi potential, is a constant related to the biosorption energy, R is the gas constant ($8.314 \text{ kJ mol}^{-1}$), and T is the absolute temperature (K). The Polanyi sorption theory assumes a fixed volume of sorption space close to the sorbent surface and the existence of a sorption potential over these spaces. The mean free energy of biosorption (E) can be calculated from the following equation:

$$E = \frac{1}{\sqrt{2K}}. \quad (7)$$

The calculated value of mean free energy of biosorption provides noteworthy information on predicting the type of biosorption process. If $E < 8 \text{ kJ mol}^{-1}$, the biosorption process is controlled by physisorption. If $E > 16 \text{ kJ mol}^{-1}$, chemisorption is the dominant factor. When E lies between 8 and 16 kJ mol^{-1} , biosorption process is due to exchange of ions [45].

The Dubinin–Radushkevich constants are calculated using the plot (Fig. 9c) and shown in Table 3. The value of the coefficient of determination was much lower than the other four isotherm models. In all the cases, the Dubinin–Radushkevich equation represents the least fit to experimental data than the other biosorption isotherms models.

Temkin isotherm

The Temkin isotherm model takes into account the interactions between biosorbent and metal ions to be biosorbed. This model is based on the assumption that the free energy of biosorption is a function of the surface coverage [46]. The model is given by the following equation

$$q_e = \frac{RT}{b_T} \ln(A_T C_e), \quad (8)$$

where there is the A_T Temkin isotherm equilibrium binding constant (L mg^{-1}), and the b_T Temkin isotherm constant (kJ mol^{-1}). The curve presented in Fig. 9d was

plotted for q_e and $\ln C_e$ and values of both constants A_T and b_T were calculated (Table 3). The model better fitted the biosorption equilibrium data next to the Langmuir and Freundlich isotherm models, respectively. Value of b_T (2.840 kJ mol⁻¹) obtained in this study indicated that the Cr(VI) biosorption on EMAP exhibits chemisorption. This supports the predictions from the Langmuir isotherm model [47].

Jovanovic isotherm

The model of an adsorption surface considered in this model is similar to that considered by the Langmuir isotherm model [48]. It is represented by another approximation for monolayer localized adsorption without lateral interactions. The Jovanovic model is represented using the following relationship

$$q_e = q_{mj} \left(1 - e^{(K_j C_e)} \right), \quad (9)$$

where K_j denotes the Jovanovic isotherm constant (L g⁻¹), and q_{mj} is the maximum adsorption capacity in Jovanovic model (mg g⁻¹). The Jovanovic model plot is shown in Fig. 9e. The maximum biosorption capacity for the studied metal ion based on the Jovanovic model (Table 3) was lower than the Langmuir maximum biosorption capacity, which is unacceptable.

Biosorption kinetic models

The kinetic biosorption data can be used to comprehend the dynamic behavior of Cr(VI) biosorption onto the EMAB in terms of the rate constant. The kinetics parameters provide vital information for designing and modeling the biosorption process. The experimental data were evaluated by pseudo-first-order, pseudo-second-order, and intraparticle diffusion models.

Pseudo-first-order kinetics

The pseudo-first-order kinetic model is known as the Lagergren equation [49]

$$\log(q_e - q_t) = \log q_e - \frac{k_1}{2.303} t, \quad (10)$$

where q_e and q_t are the amounts of metal biosorbed (mg g⁻¹) at equilibrium and at time t (min), respectively, and k_1 is the rate constant of pseudo-first-order kinetics. Figure 10 shows the plots of $\log(q_e - q_t)$ versus t for Cr(VI) biosorption onto EMAB. In the case of the pseudo-first-order model, the coefficient of determination value was found to be low in comparison to the other two kinetic models, as shown in Table 5. Furthermore, there were significant differences between the calculated and experimental uptake values, suggesting that the biosorption kinetics does not follow pseudo-first-order kinetics.

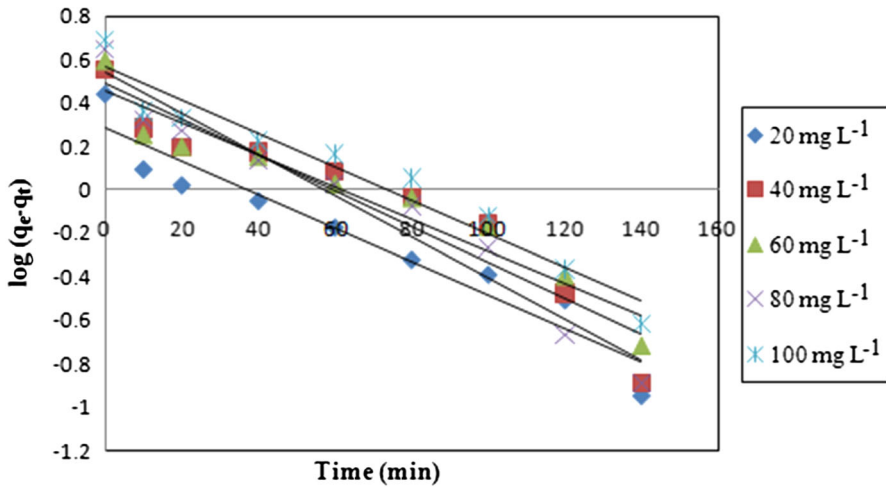


Fig. 10 Pseudo-first-order kinetics plot for biosorption of Cr(VI) by EMAB

Pseudo-second-order kinetics

The pseudo-second-order kinetic model [50] can be expressed by the following equation

$$\frac{t}{q_t} = \frac{1}{k_2 q_e^2} + \frac{t}{q_e}, \quad (11)$$

where k_2 is the rate constant for the pseudo-second-order kinetics.

The linear plots of t/q_t against t resulted in a straight line as shown in Fig. 11. The coefficient of determination value for Cr(VI) for the pseudo-second-order kinetics equation was found to be higher (Table 5). Therefore, the biosorption of Cr(VI) on EMAB follows pseudo-second-order kinetics, which is based on the assumption that chemisorption is the rate limiting step with the electron sharing and exchanging between EMAB and Cr(VI) ions [51].

Intraparticle diffusion kinetics

The intraparticle diffusion model [52] used to verify the influence of mass transfer resistance on the binding of the metal ion on the biosorbent. The intraparticle diffusion model is given in a simplified form by

$$q_t = k_{id} t^{1/2} + C, \quad (12)$$

where k_{id} is the intraparticle diffusion rate constant ($\text{mg g}^{-1} \text{min}^{-1/2}$), and C is the intercept.

Figure 12 shows the plots of q_t versus $t^{1/2}$ for EMAB and constants values of this kinetics model as represented in Table 5. The plot shows that the straight lines do

Table 5 Kinetic parameters for biosorption of Cr(VI) on EMAB

Cr(VI) conc. (mg L ⁻¹)	q_e (exp) (mg g ⁻¹)	Pseudo-first-order		Pseudo-second-order		Intraparticle diffusion				
		k_1 (min ⁻¹)	q_e (cal) (mg g ⁻¹)	R^2	k_2 (g mg ⁻¹ min ⁻¹)	q_e (cal) (mg g ⁻¹)	R^2	k_{id} (mg g ⁻¹ min ^{1/2})	C (mg g ⁻¹)	R^2
20	2.7795	0.0161	1.9186	0.920	0.0160	3.0395	0.991	0.128	1.118	0.992
40	3.5376	0.0184	3.0690	0.904	0.0077	4.0816	0.976	0.202	0.912	0.970
60	3.9156	0.0161	2.8575	0.923	0.0093	4.3478	0.984	0.188	1.424	0.979
80	4.3871	0.0207	3.4833	0.951	0.0097	4.8543	0.993	0.228	1.560	0.995
100	4.8387	0.0161	3.6728	0.943	0.0072	5.4347	0.986	0.247	1.623	0.985

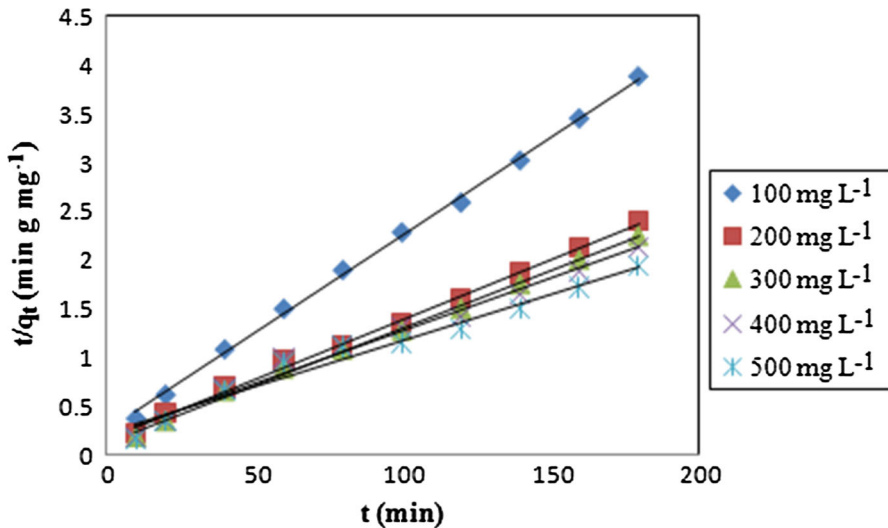


Fig. 11 Pseudo-second-order kinetic plot for biosorption of Cr(VI) on EMAB

not pass through the origin. These findings suggest that the intraparticle diffusion is not the only rate controlling step for the Cr(VI) biosorption process and some other mechanisms are involved along with intraparticle diffusion [53].

Thermodynamics of biosorption

The thermodynamic parameters include Gibbs free energy change (ΔG°), enthalpy change (ΔH°), and entropy (ΔS°) change were used to describe the thermodynamic behavior of the biosorption of Cr(VI) ions by EMAB. These parameters were determined by the following equations:

$$\Delta G^\circ = -RT \ln K_C, \quad (13)$$

$$\ln K_C = \frac{-\Delta H^\circ}{RT} + \frac{\Delta S^\circ}{R}, \quad (14)$$

where T is the absolute temperature (K) and R is the gas constant ($8.314 \text{ J mol}^{-1} \text{ K}^{-1}$) and K_C is the distribution coefficient given by

$$K_C = q_e / C_e. \quad (15)$$

Thermodynamic parameters were calculated using the plots of $\ln k_c$ versus $1/T$, and the values of ΔG° , ΔH° , and ΔS° are summarized in Table 6. The negative values of ΔG° at the temperature of 303, 313, and 323 K suggested that Cr(VI) biosorption is spontaneous in nature. The positive values of ΔH° and ΔS° indicated that the biosorption process was endothermic and increased randomness at the solid–solution interface during the fixation of the Cr(VI) ions on the active sites of the EMAB (Table 6).

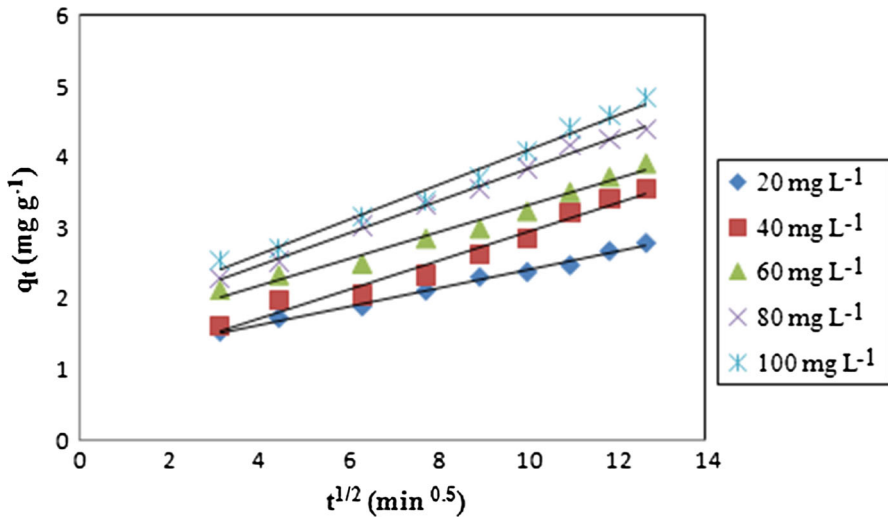


Fig. 12 Intraparticle diffusion plot of removal of Cr(VI) by EMAB

Table 6 Thermodynamic parameters for Cr(VI) biosorption on EMAB

Temperature (K)	$\ln k_c$	ΔG° (kJ mol ⁻¹)	ΔH° (kJ mol ⁻¹)	ΔS° (kJ mol ⁻¹ K ⁻¹)
303	-1.1616	-2.926	90.722	0.285
313	-1.0476	-2.726		
323	-0.0658	-0.176		
333	2.1624	5.986		

Table 7 Biosorption capacity of different biosorbents

Biosorbents	Biosorption capacity (mg g ⁻¹)	C ₀ (mg L ⁻¹)	pH	Temperature (K)	References
Coconut tree sawdust	3.46	5–20	3.0	–	[54]
<i>Acacia albida</i>	2.983	5–20	2.0	300	[55]
Sugarcane bagasse	1.76	10–140	2.0	298	[56]
<i>Borassus aethiopum</i> flower	4.9	10–150	4.5	303	[57]
Wheat bran	0.942	2.5–15	3.0	298	[58]
<i>Helianthus annuus</i>	3.6	10–70	2.0	300	[59]
<i>Peganum harmala</i>	2.31	15–100	1.5	300	[60]
<i>Enteromorpha</i> sp.	5.3475	20–100	2.0	303	Present study
<i>Ficus auriculata</i> leaves powder	13.33	20–100	2.0	303	[61]

Conclusions

The present study showed that EMAB can remove Cr(VI) by biosorption. The biosorption capacity of EMAB was compared with other biosorbents and represented in Table 7. The effect of the initial solution pH, biomass dosage, initial Cr(VI) concentration, and temperature on Cr(VI) biosorption was investigated. It was observed that the extent of biosorption increased with the lowering of pH up to 2.0. In the studied hexavalent chromium concentration range, biosorption capacities increased with increasing initial hexavalent chromium concentrations and temperatures. The two parameters in the isotherm models were used for the mathematical description of the biosorption equilibrium of Cr(VI) ions to EMAB. It was seen that the biosorption equilibrium data fitted well to the both Langmuir and Freundlich isotherms. The suitability of the pseudo-first-order, pseudo-second-order, and intraparticle diffusion kinetic models for the biosorption of Cr(VI) onto EMAB was discussed. The pseudo-second-order kinetic model agrees very well with the dynamical behavior for the biosorption of Cr(VI) onto EMAB. Thermodynamic constants were also evaluated using equilibrium constants by changing with temperature. The negative value of ΔG° indicated the spontaneity, the positive values of ΔH° and ΔS° showed the endothermic nature, and the irreversibility of the Cr(VI) biosorption process. Therefore, the abundant and the zero cost biosorbent could be used as a competent, economical, and eco-friendly biosorbent for the detoxification of Cr(VI) from aqueous solution. Further research is required to establish the activation methods in order to increase the biosorption capacity of EMAB and an approach over dynamic modeling is needed for Cr(VI) removal from industrial wastewater.

Acknowledgments Financial support from the Department of Science and Technology, India, for financial support (Grant No. SERC/ET-0356/2012) is thankfully acknowledged.

References

1. A.I. Zouboulis, M.X. Loukidou, K.A. Matis, *Process. Biochem.* **39**, 909–916 (2004)
2. M.S. Ahmed, Y. Aslam, W.A. Khan, *J. Anim. Plant Sci.* **21**, 176–181 (2011)
3. M.S. Mortazavi, S. Sharifian, *Int. J. Environ. Res.* **5**, 757–762 (2011)
4. M.S. Ahmed, S. Bibi, *J. Anim. Plant Sci.* **20**, 201–207 (2010)
5. Z.J. Kowalski, *J. Hazard. Mater.* **37**, 137–144 (1994)
6. N. Kuyucak, B. Volesky, (CRC, Boca Raton 1990), pp. 173–198
7. T. Viraraghavan, G.Y. Yan, *Bioresour. Technol.* **78**, 243–249 (2001)
8. M. Costa, *Toxicol. Appl. Pharmacol.* **188**, 1–5 (2003)
9. U.K. Garg, M.P. Kaur, V.K. Garg, D. Sud, *J. Hazard. Mater.* **140**, 60–68 (2007)
10. WHO, *Guidelines for Drinking-Water Quality* (World Health Organization, Geneva, 1993)
11. IS 10500:1991 (1991) Drinking Water Specifications. Bureau of Indian Standards, New Delhi
12. M. Owlad, M.K. Aroua, W.A.W. Daud, S. Baroutian, *Water Air Soil Pollut.* **200**, 59–77 (2009)
13. G.M. Gadd, *J. Chem. Technol. Biotechnol.* **84**, 13–28 (2009)
14. A.H. Muhammad, N. Raziya, N.B. Haq, R.A. Najum, M.A. Tariq, *J. Hazard. Mater.* **139**, 345–355 (2007)
15. V.K. Gupta, A. Rastogi, *J. Hazard. Mater.* **152**, 407–414 (2008)
16. S. Rangabhashiyam, E. Suganya, N. Selvaraju, A.V. Lity, *World J. Microbiol. Biotechnol.* **30**, 1669–1689 (2014)

17. F. Marina, M.G. Geoffrey, *Bioresour. Technol.* **160**, 3–14 (2014)
18. S. Rangabhashiyam, N. Selvaraju, *J. Taiwan Inst. Chem. Eng.* **47**, 59–70 (2015)
19. J. Cheng-guang, Z. Ya-ping, W. He, O. Guang-nan, L. Qi-ming, L. Jin-mei, *J. Cent. South Univ.* **21**, 2801–2809 (2014)
20. R. Jayakumar, M. Rajasimman, C. Karthikeyan, *J. Environ. Chem. Eng.* **2**, 1261–1274 (2014)
21. S. Rangabhashiyam, N. Selvaraju, *J. Mol. Liq.* **207**, 39–49 (2015)
22. A.E. Sikkaily, N.A. Ei, A. Khaled, O. Abdelwehab, *J. Hazard. Mater.* **148**, 216–228 (2007)
23. A.H. Moubasher, S.I.I. Abdel-Hafez, H.M. Abdel-Fattah, A.M. Moharram, *Mycopathologia* **78**, 169–176 (1982)
24. C. Namasivayam, D. Sangeetha, *J. Hazard. Mater.* **B135**, 449–452 (2006)
25. S. Sugashini, K.M. Meera, Sheriffa Begum, *Clean Technol. Environ. Policy* **15**, 293–302 (2013)
26. C. Abuzer, B. Huseyin, *Desalination* **275**, 141–147 (2011)
27. H. Lalhruiatlunga, M.N.V. Prasad, K. Radha, *Desalination* **271**, 301–308 (2011)
28. S. Gupta, B.V. Babu, *Chem. Eng. J.* **150**, 352–365 (2009)
29. V.K. Gupta, A. Rastogi, *J. Hazard. Mater.* **163**, 396–402 (2009)
30. S. Mor, R. Khaiwal, N.R. Bishnoi, *Bioresour. Technol.* **98**, 954–957 (2007)
31. D. Liping, Z. Yang, Q. Jie, W. Xinting, Z. Xiaobin, *Miner. Eng.* **22**, 372–377 (2009)
32. S. Biswajit, K.D. Sudip, *Colloids Surf. B Biointerfaces* **84**, 221–232 (2011)
33. K. Rajender, R.B. Narsi, Garima, B. Kiran, *Chem. Eng. J.* **135**, 202–208 (2008)
34. K. Meghna, K.M. Monoj, *Chem. Eng. J.* **218**, 138–146 (2013)
35. N. Abdel-Jabbar, S. Al-Asheh, *J. Environ. Protect. Sci.* **3**, 133–139 (2009)
36. G.B. Yeslie, L.R.R. Ivan, G. Eric, C.H. Monica, A.M.L. Maria, *Chem. Eng. J.* **183**, 68–76 (2012)
37. O. Sadin, K. Ersin, P. Annarita, N. Barbara, G. Kemal, *Chem. Eng. J.* **152**, 195–206 (2009)
38. X.S. Wang, L.F. Chen, F.Y. Li, K.L. Chen, W.Y. Wan, Y.J. Tang, *J. Hazard. Mater.* **175**, 816–822 (2010)
39. P. Sharma, P. Kumari, M.M. Srivastava, S. Srivastava, *Bioresour. Technol.* **98**, 474–477 (2007)
40. S. Rangabhashiyam, N. Anu, M.S. Giri Nandagopal, N. Selvaraju, *J. Environ. Chem. Eng.* **2**, 398–414 (2014)
41. I. Langmuir, *J. Am. Chem. Soc.* **38**, 2221–2229 (1916)
42. H. Freundlich, *Z. Phys. Chem.* **40**, 1361–1368 (1906)
43. A. Gunay, E. Arslankaya, I. Tosun, *J. Hazard. Mater.* **146**, 362–371 (2007)
44. M.M. Dubinin, L.V. Radushkevich, *Proc. Acad. Sci. USSR* **55**, 331–333 (1947)
45. M. Ghasemi, M. Naushad, N. Ghasemi, Y. Khosravi-fard, *J. Ind. Eng. Chem.* **20**, 2193–2199 (2014)
46. M.I. Temkin, V. Pyzhev, *Acta Physicochim. USSR* **12**, 217–222 (1940)
47. S. Aytas, D.A. Turkozu, C. Gok, *Desalination* **280**, 354–362 (2011)
48. D.S. Jovanovic, *Colloid Polym. Sci.* **235**, 1203–1214 (1969)
49. S. Lagergerm, About the theory of so-called adsorption of soluble substances. *K. Sven. Vetenskap-sakad. Handl.* **2**, 1–39 (1898)
50. Y.S. Ho, G. McKay, *Chem. Eng. J.* **70**, 115–124 (1998)
51. Z. Jinghui, F. Hao, L. Xiaoshu, T. Jie, X. Xinhua, *Biomass Bioenergy* **35**, 464–472 (2011)
52. W. Weber, J. Morris, *J. Sanit. Eng. Div. ASCE* **89**, 31–60 (1963)
53. A.C.A. Lima, R.F. Nascimento, F.F. Sousa, M.F. Josue, C.O. Alcinea, *Chem. Eng. J.* **185–186**, 274–284 (2012)
54. K. Selvi, S. Pattabhi, K. Kadirvelu, *Bioresour. Technol.* **80**, 87–89 (2001)
55. G. Gebrehawaria, A. Hussen, V.M. Rao, *Int. J. Environ. Sci. Technol.* (2014). doi:[10.1007/s13762-014-0530-2](https://doi.org/10.1007/s13762-014-0530-2)
56. I.C. Aloma, I. Rodriguez, M. Calero, G. Blazquez, *Desalin. Water Treat.* **52**, 5912–5922 (2014)
57. R. Elangovan, L. Philip, K. Chandraraj, *Chem. Eng. J.* **141**, 99–111 (2008)
58. M. Nameni, M.R.A. Moghadam, M. Arami, *Int. J. Environ. Sci. Technol.* **5**, 161–168 (2008)
59. M. Jain, V.K. Garg, K. Kadirvelu, *J. Hazard. Mater.* **162**, 365–372 (2009)
60. R. Khosravi, M. Fazlzadehdavil, B. Barikbin, A.A. Taghizadeh, *Appl. Surf. Sci.* **292**, 670–677 (2014)
61. S. Rangabhashiyam, E. Nakkeeran, N. Anu, N. Selvaraju, *Res. Chem. Intermed.* (2014). doi:[10.1007/s11164-014-1900-6](https://doi.org/10.1007/s11164-014-1900-6)